Journal of the Physical Society of Japan
Vol. 73, No. 8, August, 2004, pp. 2283–2291

A-site Randomness Effect on Structural and Physical Properties of Ba-based Perovskite Manganites

Tomohiko NAKAJIMA*, Hideki YOSHIZAWA[1] and Yutaka UEDA

Materials Design and Characterization Laboratory, Institute for Solid State Physics, University of Tokyo, 5-1-5 Kashiwanoha, Kashiwa, Chiba 277-8581
[1]*Neutron Science Laboratory, Institute for Solid State Physics, University of Tokyo, 106-1 Shirakata, Tokai, Ibaraki 319-1106*

(Received April 14, 2004)

The discovery of novel structural and physical properties in the *A*-site ordered manganite RBaMn$_2$O$_6$ (R = Y and rare earth elements) has demanded new comprehension about perovskite manganese oxides. In the present study, the *A*-site disordered form, $R_{0.5}$Ba$_{0.5}$MnO$_3$, has been investigated and compared with both RBaMn$_2$O$_6$ and $R_{0.5}A_{0.5}$MnO$_3$ (*A*: Sr, Ca) in the structures and electromagnetic properties. $R_{0.5}$Ba$_{0.5}$MnO$_3$ has a primitive cubic perovskite cell in the structure and magnetic glassy states are dominant as its ground state, in contrast to the ordinary disordered $R_{0.5}A_{0.5}$MnO$_3$ (*A*: Sr, Ca). In Pr-compounds with various degrees of Pr/Ba randomness at the *A*-sites, the *A*-site disorder gradually suppresses both ferromagnetic and A-type antiferromagnetic transitions and finally leads to a magnetic glassy state in Pr$_{0.5}$Ba$_{0.5}$MnO$_3$. A peculiar behavior, multi-step magnetization and resistivity change, has been observed in Pr$_{0.5}$Ba$_{0.5}$MnO$_3$. These properties could be closely related to any spatial heterogeneity caused by the random distribution of Ba^{2+} and R^{3+} with much different ionic radius.

KEYWORDS: A-site ordered/disordered perovskite manganites, crystal structure, electromagnetic properties, randomness effect, magnetoresistance effect
DOI: 10.1143/JPSJ.73.2283

1. Introduction

The magnetic and electrical properties of perovskite manganites with the general formula $(R^{3+}_{1-x}A^{2+}_x)$MnO$_3$ (R = rare earth elements and A = Ca and Sr) have been extensively investigated for the last decade.[1)] Among the interesting features are the so-called colossal magnetoresistance (CMR) and metal–insulator (MI) transition accompanied by charge/orbital order (CO). It is now widely accepted that these enchanting phenomena are caused by the strong correlation/competition among spin, charge and orbital degrees of freedom, which would be significantly influenced by the *A*-site randomness. Recently we successfully synthesized the *A*-site ordered manganite, RBaMn$_2$O$_6$ (R = Y and rare earth elements) and reported its structure and electromagnetic properties.[2–6)] As schematically shown in Fig. 1, the most significant structural feature of RBaMn$_2$O$_6$ is that the MnO$_2$ square sublattice is sandwiched by two types of rock-salt layers, *R*O and BaO, with much different sizes, and consequently the MnO$_6$ octahedron itself is distorted in a noncentrosymmetric manner that both Mn and oxygen atoms in the MnO$_2$ plane are displaced toward the *R*O layer [Fig. 1(c)], in contrast to the rigid MnO$_6$ octahedron in the *A*-site disordered manganite $(R_{1-x}A_x)$MnO$_3$ (A = Ca and Sr). This means that the structural and physical properties of RBaMn$_2$O$_6$ can be no longer explained in terms of the basic structural distortion, the so-called tolerance factor f, as can be in $(R_{0.5}A_{0.5})$MnO$_3$ (A = Ca and Sr).[1)] Figure 2 shows the electronic phase diagram of RBaMn$_2$O$_6$ expressed as a function of the ratio of ionic radius of the *A*-site cations.[3)] Among possible combinations of R/Ba, the mismatch between *R*O and BaO is the smallest in La/Ba and the

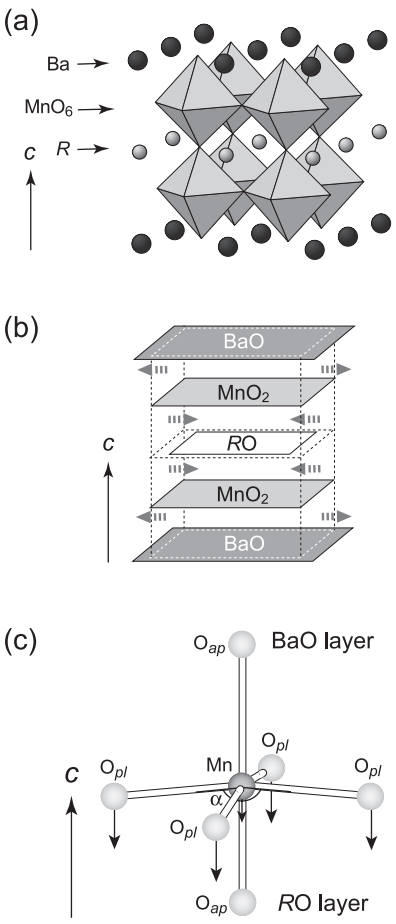

Fig. 1. (a) Crystal structure and (b) structural concept of the *A*-site ordered manganite RBaMn$_2$O$_6$, and (c) an illustration of the distorted MnO$_6$ octahedron.

*Present address: Materials Design and Characterization Laboratory, Institute for Solid State Physics, University of Tokyo, 5-1-5 Kashiwanoha, Kashiwa, Chiba 277-8581.

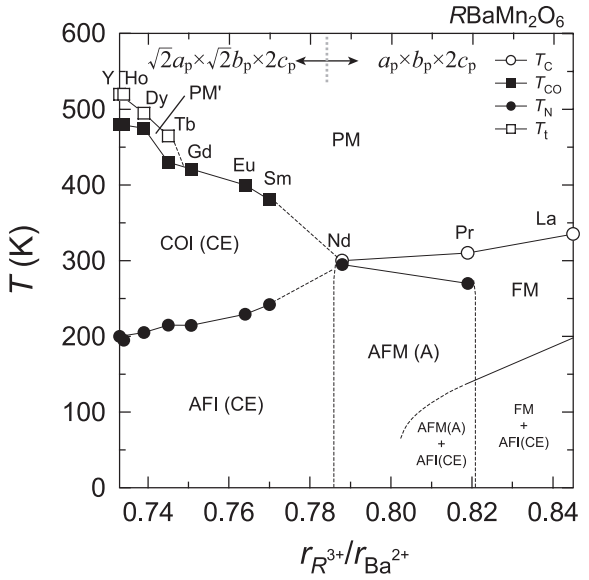

Fig. 2. Electronic phase diagram for the *A*-site ordered manganite RBaMn$_2$O$_6$. PM (PM′): paramagnetic metal phase, FM: ferromagnetic metal phase, AFM(A): A-type antiferromagnetic metal phase, COI(CE): CE-type charger/orbital ordered insulator phase, AFI(CE): CE-type antiferromagnetic insulator phase.

largest in Y/Ba. As seen in Fig. 2, the CE-type charge/orbital ordered state [COI(CE)] with a new stacking variation of the CE-type CO is stabilized at the relatively high temperatures (T_{CO}) far above 300 K, when R^{3+} is smaller than Sm^{3+} in ion size. The high T_{CO} would be not only due to the absence of *A*-site randomness but also due to the distorted structure with a tilt of MnO_6 octahedra as well as heavy distortion of MnO_6 octahedron.[5] The new CE-type CO with a 4-fold periodicity along the *c*-axis (4CE-CO) could be due to a layer type order of *R* and Ba.[4] Interestingly, this 4CE-CO changes into a new type with a two or single periodicity along the *c*-axis, when the system enters into the antiferromagnetic CE-type charge/orbital ordered state [AFI(CE)].[4] Furthermore, RBaMn$_2$O$_6$ (R = Tb, Dy, Ho and Y) shows the structural transition at T_t above T_{CO}, as shown in Fig. 2, which is possibly accompanied by a $d_{x^2-y^2}$ type orbital order.[3,5] Therefore the degeneracy of orbital, charge and spin degrees of freedom are lifted in these compounds. On the other hand, RBaMn$_2$O$_6$ (R = La, Pr and Nd) with relatively larger R^{3+} has no octahedral tilt and shows a transition from a paramagnetic metal (PM) to a ferromagnetic metal (FM). The ground states for PrBaMn$_2$O$_6$ and NdBaMn$_2$O$_6$ are the A-type antiferromagnetic metal [AFM(A)]. In LaBaMn$_2$O$_6$, AFI(CE) phase coexists with FM phase in the ground state, which suggests that the electronic phase separation is not due to the *A*-site randomness but is intrinsic phenomenon in perovskite manganites where FM and CO interactions compete against each other and are significantly influenced by a tiny change of the local structure.[6]

The discovery of such novel structural and physical properties in the *A*-site ordered manganite RBaMn$_2$O$_6$ has demanded new comprehension about perovskite manganese oxides.[3–11] Recently, theoretical studies also have revealed that the interesting properties such as CMR and electronic phase separation come from a critical competition between FM and an antiferromagnetic CO interaction, which could be significantly influenced by the *A*-site randomness or a fluctuation of the local structure[12,13] The *A*-site disordered form ($R_{0.5}$Ba$_{0.5}$)MnO$_3$ with the same constituent elements is crucial to deepen the understanding of the structural and physical properties of perovskite manganites; it may make clear the effects of *A*-site randomness not only qualitatively but also quantitatively. Very recently Akahoshi *et al.* reported that the magnetic glassy state became dominant in ($R_{0.5}$Ba$_{0.5}$)MnO$_3$.[11] However the detailed structure and electromagnetic properties of ($R_{0.5}$Ba$_{0.5}$)MnO$_3$ has not been reported. We have also independently synthesized the *A*-site disordered Ba-based manganite ($R_{0.5}$Ba$_{0.5}$)MnO$_3$ and studied the structure and electromagnetic properties in terms of the degree of *A*-site randomness. In this paper, we report the structures and electromagnetic properties of ($R_{0.5}$Ba$_{0.5}$)-MnO$_3$, especially Pr-compounds with various degrees of the randomness of Pr/Ba at the *A*-sites, and we will discuss the obtained results in terms of the *A*-site randomness effect.

2. Experimental

Polycrystalline samples of ($R_{0.5}$Ba$_{0.5}$)MnO$_3$ (R = Y and rare earth elements) were prepared by a solid-state reaction of R_2O_3, BaCO$_3$ and MnO$_2$ at 1623 K in 1% O$_2$/Ar gas for 1 day, followed by annealing at 1173 K in O$_2$ gas for 1 day (Path I in Fig. 3). The preparation method of the ordered form RBaMn$_2$O$_6$ was reported elsewhere.[2,3,5] Interestingly, annealing RBaMn$_2$O$_6$ under O$_2$ gas at high temperatures always resulted in insufficient R/Ba solid-solution at the *A*-sites. Pr-compounds: $[Pr_gBa_{1-g}]_P[Pr_{1-g}Ba_g]_BMn_2O_6$ ($0.5 \leq g \leq 1.0$) with various degrees of the *A*-site order were synthesized from PrBaMn$_2$O$_6$ by controlling the annealing time and temperatures (1273–1623 K) in O$_2$ gas (Path II in Fig. 3), where [ ]$_P$ (or [ ]$_B$) represents Pr-sites (or Ba-sites) in PrBaMn$_2$O$_6$. The degree of *A*-site order (*S*), $S = (2g - 1) \times 100\%$, was determined by the Rietveld analysis of powder X-ray and neutron diffractions. We obtained $S = 96 \pm 2\%$ for the ordered form PrBaMn$_2$O$_6$ and $S = 0.0\%$ for the disordered form Pr$_{0.5}$Ba$_{0.5}$MnO$_3$ prepared by Path I in Fig. 3. In the present study, we successfully prepared Pr-compounds: $[Pr_gBa_{1-g}]_P[Pr_{1-g}Ba_g]_BMn_2O_6$ ($0.5 \leq g \leq 1.0$) with S = 96(2)%, 87(4)%, 70(4)%, 57(6)%, 32(2)%, 25(6)% and 0.0% which were named as PB96, PB87, PB70, PB57,

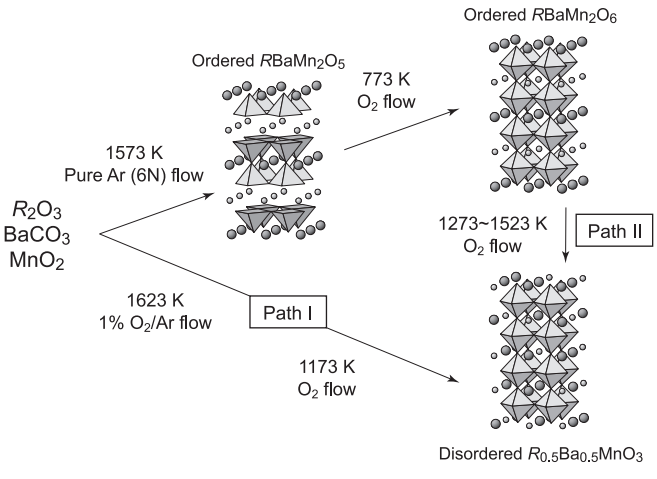

Fig. 3. Flowchart of sample preparation.

Table I. Synthesis conditions of Pr-compounds (PB96–PB00) with various degrees of the *A*-site randomness. (See the text).

Sample	Synthesis condition
PB96	Heating starting materials at 1623 K in pure Ar for 24 h, followed by annealing at 623 K in O_2 for 24 h
PB87	Annealing PB96 at 1273 K in O_2 for 6 h
PB70	Annealing PB87 at 1523 K in O_2 for 24 h
PB57	Annealing PB70 at 1523 K in O_2 for 24 h
PB32	Annealing PB57 at 1623 K in O_2 for 24 h
PB25	Annealing PB32 at 1623 K in O_2 for 24 h
PB00	Heating starting materials at 1623 K in 1% O_2/Ar for 24 h, followed by annealing at 1173 K in O_2 for 24 h

PB32, PB25 and PB00, respectively. The synthesis conditions of these Pr-compounds are shown in Table I.

The crystal structures including the order/disorder of *R*/Ba were refined by the Rietveld analysis of powder X-ray and neutron diffractions using RIETAN 2000.[14] The magnetic ordered states at low temperatures were studied by powder neutron diffraction. The X-ray powder diffraction experiments were performed using a MXP21 Mac Science diffractometer with the following operation conditions: $5^\circ < 2\theta < 120^\circ$ with the step size of 0.02°, Cu Kα radiation, $V = 45$ kV and $I = 350$ mA. The powder neutron diffraction was performed with the Kinken powder diffractometer, HERMES, of Institute for Materials Research (IMR), Tohoku University, installed at the JRR-3M reactor in Japan Atomic Energy Research Institute (JAERI), Tokai. Neutrons with a wavelength of 1.8207 Å were obtained by the 331 reflection of the Ge monochromator and the 12′-blank-sample-22′ collimation. The magnetic properties were studied using a SQUID magnetometer in a temperature range $T = 2$–400 K. The electric resistivity of a sintered pellet was measured for $T = 2$–400 K by a conventional four-probe technique.

3. Results and Discussion

3.1 The A-site disordered $R_{0.5}Ba_{0.5}MnO_3$

The X-ray diffraction patterns of all $R_{0.5}Ba_{0.5}MnO_3$ can be indexed in the primitive cubic perovskite cell. There is no extra peak suggesting a superstructure. The lattice parameters of $R_{0.5}Ba_{0.5}MnO_3$ at room temperature are shown in Fig. 4. The lattice parameter decreases with decreasing ionic radius of R^{3+}. The simple cubic cell means no tilt of MnO_6 octahedra in contrast to the orthorhombic $GdFeO_3$ type distortion of $R_{0.5}A_{0.5}MnO_3$ (A = Ca and Sr). In general, the mismatch between the larger MnO_2 and the smaller $(R,A)O$ sublattices is relaxed by tilting MnO_6 octahedra, resulting in the lattice distortion from cubic to, mostly, the orthorhombic $GdFeO_3$-type structure. In this distortion, the bond angle $\angle$Mn-O-Mn deviates from 180°, leading to a significant change in the effective one-electron bandwidth or equivalent e_g-electron transfer interaction, and the degree of this mismatch is described as $f = (\langle r_A \rangle + r_O)/\sqrt{2}[(r_{Mn} + r_O)]$, where $\langle r_A \rangle$, r_{Mn} and r_O are (averaged) ionic radii for the respective elements. The electronic phase diagram of $R_{0.5}A_{0.5}MnO_3$ (A = Ca and Sr) has been explained by f; FM state generated by the double-exchange interaction is dominant near $f = 1$, while COI(CE) state is most stabilized

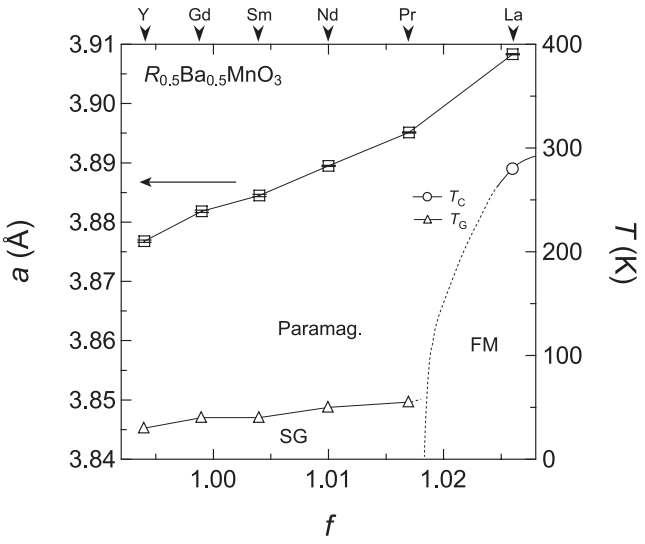

Fig. 4. Lattice parameters at room temperature and phase diagram of the *A*-site disordered $R_{0.5}Ba_{0.5}MnO_3$ as a function of the tolerance factor f. SG: spin glass phase.

in the lower f region ($f < 0.975$).[1] In $R_{0.5}Ba_{0.5}MnO_3$, the f is in the range from 1.026 (La/Ba) to 0.995 (Y/Ba), which are rather close to $f = 1$, comparing to the variation $0.955 < f < 1$ in $R_{0.5}A_{0.5}MnO_3$ (A = Ca and Sr).[15] Therefore the simple cubic structures of $R_{0.5}Ba_{0.5}MnO_3$ can be partly understood from the f-values close to 1, that is relatively small mismatch between MnO_2 and $(R_{0.5}Ba_{0.5})O$ lattices. Here, it should be noticed that the f is beyond 1 in $R_{0.5}Ba_{0.5}MnO_3$ (R = La, Pr and Nd). Actually the lattice parameters (3.904–3.918 Å)[6] of these compounds are larger than the ideal one (~3.89 Å)[15] of $Mn^{3.5+}O_2$ lattice. From simple cubic structures of $R_{0.5}Ba_{0.5}MnO_3$, one may expect FM generated by double exchange interaction as the stable electronic state. The ground state of $La_{0.5}Ba_{0.5}MnO_3$ is actually a pure FM and the ferromagnetic transition temperature T_C decreases by 50 K compared with $T_C = 330$ K in $LaBaMn_2O_6$, agreeing with the previous report.[7] On the other hand, $Pr_{0.5}Ba_{0.5}MnO_3$ and $Nd_{0.5}Ba_{0.5}MnO_3$ show the increase of magnetic susceptibility (M/H) below about 150 K and then show glassy behaviors below about 50 K, evidenced by significant differences of M/H–T curves on zero-field cooled (ZFC) and field cooled (FC) processes. As an example, the M/H–T curve for $Nd_{0.5}Ba_{0.5}MnO_3$ is shown in Fig. 5(a), together with that for $NdBaMn_2O_6$. Akahoshi *et al.*[11] previously reported FM states for $Pr_{0.5}Ba_{0.5}MnO_3$ and $Nd_{0.5}Ba_{0.5}MnO_3$, which could be due to imperfect disorder as verified in the following section of this paper. More typical spin-glass behaviors have been observed in $R_{0.5}Ba_{0.5}MnO_3$ with Sm^{3+} and smaller R^{3+}s, agreeing with the previous report.[11] The typical M/H–T curves of $Sm_{0.5}Ba_{0.5}MnO_3$ and $Y_{0.5}Ba_{0.5}MnO_3$ are shown in Fig. 5(b) and 5(c) together with those for $SmBaMn_2O_6$ and $YBaMn_2O_6$. $YBaMn_2O_6$ particularly shows three successive transitions; the structural transition at T_t, CO transition at T_{CO} and antiferromagnetic transition at T_N.[2,3,5] The magnetic interaction is ferromagnetic above T_t, while below T_t it is antiferromagnetic.[2,3,5] In $Y_{0.5}Ba_{0.5}MnO_3$, on the other hand, there is no evidence or no trace of the transitions observed in $YBaMn_2O_6$, except for the spin-glass (SG)

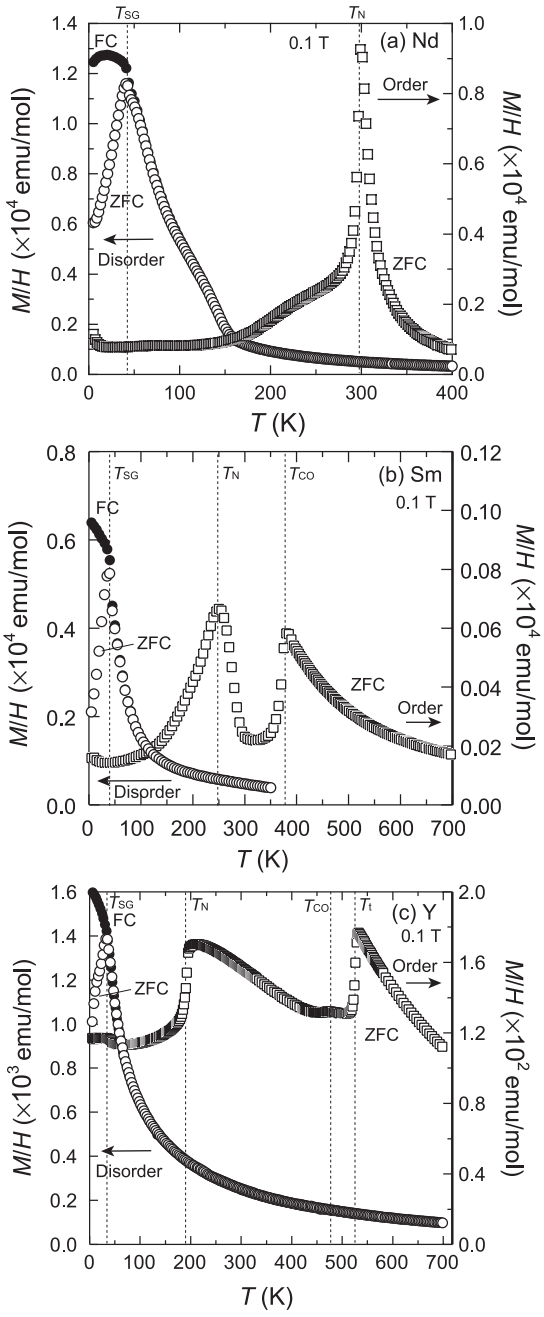

Fig. 5. Temperature dependence of magnetic susceptibility for the *A*-site ordered/disordered (a) $NdBaMn_2O_6/Nd_{0.5}Ba_{0.5}MnO_3$, (b) $SmBaMn_2O_6/Sm_{0.5}Ba_{0.5}MnO_3$ and (c) $YBaMn_2O_6/Y_{0.5}Ba_{0.5}MnO_3$ under 0.1 T.

transition at $T_G = 30$ K. The electrical resistivities of $R_{0.5}Ba_{0.5}MnO_3$ (R = Nd, Sm and Y) show semiconductive behaviors, as shown in Fig. 6. The activation energy E_a decreases with decreasing the ionic radius of R^{3+} ion.

The results of magnetic properties of $R_{0.5}Ba_{0.5}MnO_3$ are summarized in Fig. 4 as the phase diagram. Here we compare the phase diagram among $RBaMn_2O_6$, $R_{0.5}Ba_{0.5}MnO_3$ and $R_{0.5}A_{0.5}MnO_3$ (A = Ca and Sr). The electronic states characteristic of perovskite manganites such as AFM(A) and COI(CE) seen in $RBaMn_2O_6$ and $R_{0.5}A_{0.5}MnO_3$ (A = Ca and Sr) are absent in $R_{0.5}Ba_{0.5}MnO_3$. Instead of these states, magnetic glassy states govern the electronic state of $R_{0.5}Ba_{0.5}MnO_3$. The magnetic glassy state could be due to a disorder effect that hinders magnetic long-range ordering and it could occur as a result of the competition

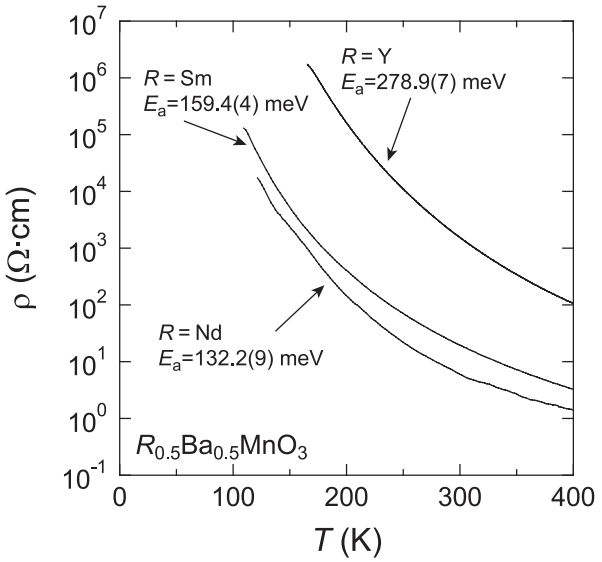

Fig. 6. Temperature dependence of resistivity for the sintered $R_{0.5}Ba_{0.5}MnO_3$ (R = Nd, Sm and Y) sample.

between randomly distributed ferromagnetic and antiferromagnetic interactions. Since the ionic radius of Ba^{2+} (= 1.61 Å)[15] is much larger than that of Sr^{2+} (= 1.44 Å)[15] and R^{3+} (≤1.36 Å),[15] $R_{0.5}Ba_{0.5}MnO_3$ could include any spatial heterogeneity in a nanometer scale, which results in magnetic nonhomogeneous states. Only the largest La^{3+} among R^{3+}s forms a homogeneous solid-solution at the *A*-sites with Ba^{2+} and the magnetic long-range ordering of FM is realized in $La_{0.5}Ba_{0.5}MnO_3$.

It has been suggested that the electromagnetic properties of perovskite manganites with *A*-site cations randomly distributed depend on not only f but also the variance of *A*-cation radius distribution σ^2 defined as $\sigma^2 = \sum y_i r_i^2 - r_A^2$, where r_i is the ionic radius of each *A*-site cation, y_i is the fractional occupancy of the i ion, r_A is the average ionic radius of *A*-site cations.[16] The value of σ^2 indicates the magnitude of potential disorder effect. Here, we discuss the ground states of the *A*-site disordered systems $R_{0.5}A_{0.5}MnO_3$ (A = Ca, Sr and Ba) in terms of σ^2. Figure 7 shows the mapping of $R_{0.5}A_{0.5}MnO_3$ (A = Ca, Sr and Ba) on a $\sigma^2 - \langle r_A \rangle$ diagram. The data of $R_{0.5}A_{0.5}MnO_3$ (A = Sr and Ca) are quoted from the previous literatures.[1,17] The thick lines in Fig. 7 represent possible phase boundaries. The magnetic long-range orderings (AFI, AFM and FM) tend to be stabilized in the lower σ^2 region ($\sigma^2 < 10^{-2}$); otherwise, the magnetic glassy state is obviously dominant above $\sigma^2 = 10^{-2}$, except FM in $La_{0.5}Ba_{0.5}MnO_3$. Thus the difference of the ionic radius between *A*-site cations significantly influences magnetic long-range ordering in perovskite manganites. In connection with the disordered effect, the lowering of both T_C and T_{CO} in the critical region is not recognized in the phase diagram of $RBaMn_2O_6$ in contrast to $R_{0.5}A_{0.5}MnO_3$ (A = Sr and Ca). The absence of such critical behavior in $RBaMn_2O_6$ is partly due to the *A*-site ordering. In the critical region where FM (AFM) and CO interactions compete against each other, they are significantly affected by fluctuation of composition, coherent size of crystal and external field etc, that is the *A*-site randomness, and such fluctuation of interactions enhances the criticality. On the

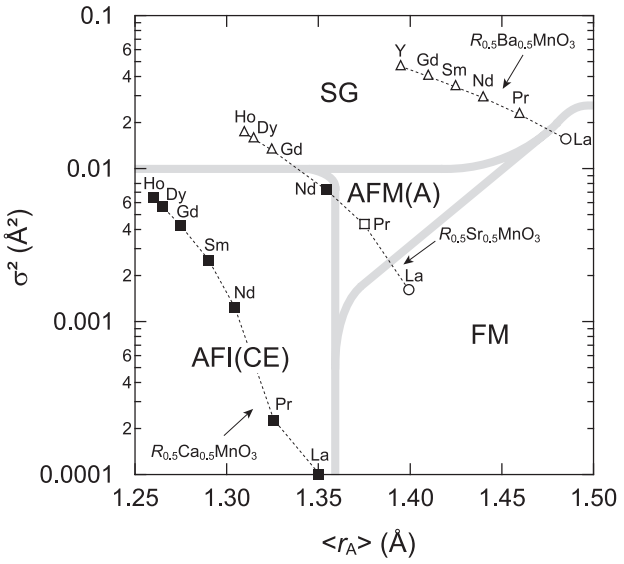

Fig. 7. A mapping of $R_{0.5}A_{0.5}MnO_3$ (A = Ca, Sr and Ba) on a $\sigma^2 - \langle r_A \rangle$ diagram. (See the text.)

other hand, it could be more definite in the A-site ordered $R BaMn_2O_6$ which interaction becomes dominant or which electronic state is stable.

3.2 *The A-site randomness effect in Pr-compounds*

As mentioned above, the structure and electromagnetic properties of perovskite manganites are significantly affected by the A-site disorder. In this section, we report the relation between those and the degree of the A-site disorder in Pr-compounds (PB96–PB00) with various degrees of the A-site randomness. Figure 8 shows X-ray diffraction patterns of the A-site ordered $PrBaMn_2O_6$ (PB96) and disordered $Pr_{0.5}Ba_{0.5}MnO_3$ (PB00). The X-ray diffraction pattern can be indexed in a simple tetragonal $P4/mmm$ for PB96–PB25 and a simple cubic $Pm\bar{3}m$ for PB00. All of them show no

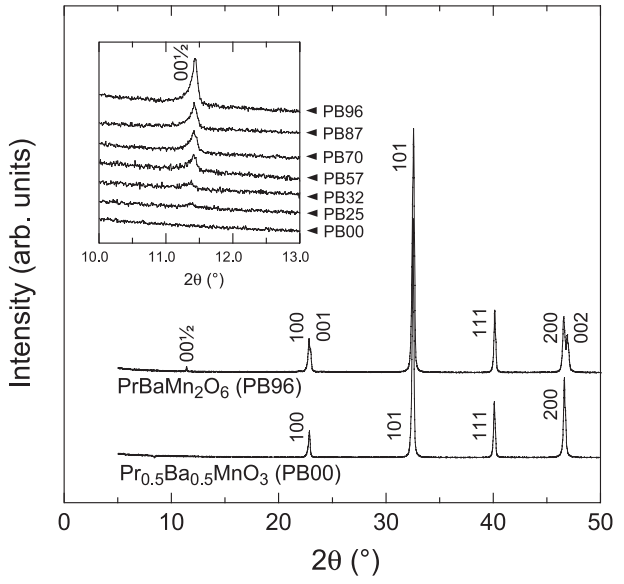

Fig. 8. X-ray diffraction patterns of the A-site ordered $PrBaMn_2O_6$ (PB96) and disordered $Pr_{0.5}Ba_{0.5}MnO_3$ (PB00). The inset shows $(00\frac{1}{2})_p$ reflections of Pr-compounds (PB96–PB00) with various degrees of Pr/Ba randomness at the A-sites.

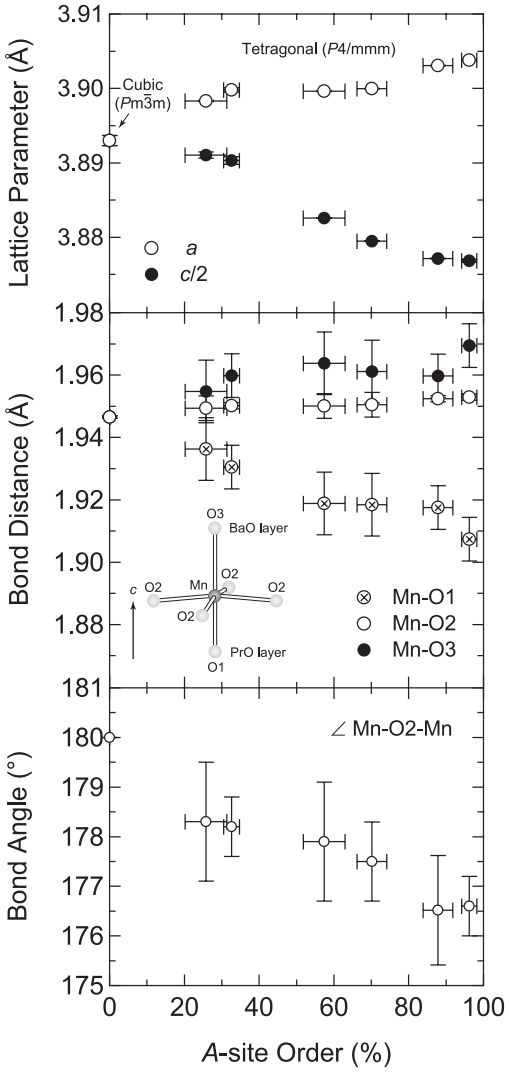

Fig. 9. Structural parameters at room temperature plotted as a function of the degree of the A-site order (%) for Pr-compounds (PB96–PB00).

trace of impurity or phase separation. The inset shows the $(00\frac{1}{2})_p$ reflections of Pr-compounds (PB96–PB00). The intensity of $(00\frac{1}{2})_p$ reflection decreases with increasing the A-site randomness and finally it becomes undetectable in PB00. Table II and Fig. 9 show the structure data of Pr-compounds. The lattice parameters, a and $c/2$, gradually approach each other with increasing the degree of the A-site disorder and terminate to the a-parameter of cubic PB00. In PB96, MnO_6 octahedra are heavily distorted in a manner as shown in Fig. 9(b); the apical Mn–O(1) distance is quite short (1.907 Å), while the other apical Mn–O(3) distance is long (1.969 Å), as a result of the displacement of MnO_2 plane toward to PrO layer. On the other hand the planar Mn–O(2) distance (1.952 Å) is close to the average length of $Mn^{3.5+}$–O bond for conventional perovskite manganites. With increasing the A-site disorder, MnO_6 octahedra gradually approach to regular octahedra.

The magnetic susceptibilities (M/H) of Pr-compounds measured under 0.1 T are shown in Fig. 10(a). PB96 shows FM transition at $T_C = 303$ K, followed by AFM(A) transition at $T_N = 245$ K. With increasing the A-site randomness, both T_C and T_N slightly decrease and AFM(A) transitions become broad. Furthermore some amount of FM state

Table II. Refined structural parameters Pr-compounds (PB96–PB00) with various degrees of the *A*-site randomness. (See the text.)

Sample		PB96	PB96	PB87	PB70	PB57
Data Resource		X-ray	Neutron	X-ray	X-ray	X-ray
Space Group		$P4/mmm$	$P4/mmm$	$P4/mmm$	$P4/mmm$	$P4/mmm$
a (Å)		3.9038(1)	3.9029(1)	3.90309(5)	3.89998(5)	3.89961(5)
c (Å)		7.7537(4)	7.7547(5)	7.75432(8)	7.7589(1)	7.7651(1)
g		0.98(1)	0.98(1)	0.93(2)	0.85(2)	0.78(3)
Pr/Ba at $[\ ]_P$	1a	$B_{iso} = 0.8(1)/0.5$	$B_{iso} = 0.8(1)/0.6$	$B_{iso} = 0.9(1)/0.6$	$B_{iso} = 0.9(1)/0.5$	$B_{iso} = 0.9(1)/0.6$
Pr/Ba at $[\ ]_B$	1b	$B_{iso} = 0.5(1)/0.8$	$B_{iso} = 0.6(1)/0.8$	$B_{iso} = 0.6(1)/0.9$	$B_{iso} = 0.5(1)/0.9$	$B_{iso} = 0.6(1)/0.9$
Mn	2h	$z = 0.2460(7)$	$z = 0.2463(6)$	$z = 0.2472(9)$	$z = 0.247(1)$	$z = 0.247(2)$
		$B_{iso} = 0.2(1)$	$B_{iso} = 0.25(8)$	$B_{iso} = 0.2(1)$	$B_{iso} = 0.3(1)$	$B_{iso} = 0.2(1)$
O1	1c	$B_{iso} = 1.0(1)$	$B_{iso} = 0.9(1)$	$B_{iso} = 1.0(1)$	$B_{iso} = 1.1(1)$	$B_{iso} = 1.1(1)$
O2	4i	$z = 0.2386(4)$	$z = 0.2385(3)$	$z = 0.239(1)$	$z = 0.241(1)$	$z = 0.242(2)$
		$B_{iso} = 1.0(1)$	$B_{iso} = 1.0(1)$	$B_{iso} = 1.0(1)$	$B_{iso} = 1.1(1)$	$B_{iso} = 1.1(1)$
O3	1d	$B_{iso} = 1.0(1)$	$B_{iso} = 1.0(1)$	$B_{iso} = 1.0(1)$	$B_{iso} = 1.1(1)$	$B_{iso} = 1.1(1)$
R_{wp} (%)		10.29	8.95	12.02	13.68	12.40
R_e (%)		7.75	6.79	8.64	9.02	8.71
A-site Order (%)		96(2)	96(2)	87(4)	70(4)	57(6)
Sample		PB57	PB32	PB32	PB25	PB00
Data Resource		Neutron	X-ray	Neutron	X-ray	X-ray
S.G.		$P4/mmm$	$P4/mmm$	$P4/mmm$	$P4/mmm$	$Pm\bar{3}m$
a (Å)		3.8997(1)	3.8998(3)	3.8996(2)	3.89829(9)	3.8930(7)
c (Å)		7.7658(3)	7.7806(8)	7.7806(5)	7.7820(4)	
g		0.79(2)	0.66(1)	0.64(1)	0.63(3)	0.5
Pr/Ba at $[\ ]_P$	1a	$B_{iso} = 0.8(1)/0.4$	$B_{iso} = 0.9(1)/0.6$	$B_{iso} = 0.8(1)/0.5$	$B_{iso} = 0.9(1)/0.6$	Pr/Ba 1a
Pr/Ba at $[\ ]_B$	1b	$B_{iso} = 0.4(1)/0.8$	$B_{iso} = 0.6(1)/0.9$	$B_{iso} = 0.5(1)/0.8$	$B_{iso} = 0.6(1)/0.9$	$B_{iso} = 0.8(1)/0.6(1)$
Mn	2h	$z = 0.2474(7)$	$z = 0.248(2)$	$z = 0.2478(8)$	$z = 0.249(1)$	Mn 1b
		$B_{iso} = 0.29(8)$	$B_{iso} = 0.2(1)$	$B_{iso} = 0.2(1)$	$B_{iso} = 0.3(1)$	$B_{iso} = 0.31(7)$
O1	1c	$B_{iso} = 1.2(1)$	$B_{iso} = 1.1(1)$	$B_{iso} = 1.1(1)$	$B_{iso} = 1.0(1)$	
O2	4i	$z = 0.2422(9)$	$z = 0.2440(7)$	$z = 0.2439(7)$	$z = 0.245(1)$	O 3c
		$B_{iso} = 1.2(1)$	$B_{iso} = 1.1(1)$	$B_{iso} = 1.1(1)$	$B_{iso} = 1.0(1)$	$B_{iso} = 1.2(1)$
O3	1d	$B_{iso} = 1.2(1)$	$B_{iso} = 1.1(1)$	$B_{iso} = 1.1(1)$	$B_{iso} = 1.0(1)$	
R_{wp} (%)		10.09	11.32	9.65	12.05	10.69
R_e (%)		6.99	8.59	6.41	9.27	8.65
A-site Order (%)		58(4)	32(2)	29(2)	25(6)	0

The degree of *A*-site order (S) is defined by $(2g - 1) \cdot 100$ (%), where g is the refined occupancy factor represented as $[Pr_gBa_{1-g}]_P[Pr_{1-g}Ba_g]_BMn_2O_6$; $[\ ]_P$ and $[\ ]_B$ show Pr-sites and Ba-sites in $PrBaMn_2O_6$, respectively.

coexists with AFM(A) state below T_N in PB87 and PB70, which is evidenced by a considerable amount of temperature independent M/H below T_N. On the other hand, PB32 and PB25 with a considerable *A*-site disorder exhibit clear FM transitions at $T_C = 158$ K and 152 K, respectively. Since the saturated values of M/H of PB32 and PB25 are lower than that expected from full moment, any short-range magnetic ordered phase and/or AFM(A) phase coexist with FM phase. The rather low T_Cs for the second group (PB32 and PB25) compared with T_Cs for the first group (PB96–PB70) suggests two types of FM phase in Pr-compounds. This might be reflected in the M/H–T curve with two peaks around 200 K and 180 K for the intermediate compound PB57, namely PB57 includes two FM phases and each FM phase transforms to AFM(A) phase at independent temperatures (200 K and 180 K), showing peaks in M/H–T curve. Finally, the perfect disordered PB00 has a much smaller M/H than that of other compounds and shows a spin glass like transition at 50 K, as shown in the inset of Fig. 10(a). A small amount of AFM(A) phase was confirmed at low temperature by a neutron diffraction measurements, but FM long-range ordered phase was not observed.

The obtained results of Pr-compounds are summarized in Fig. 10(b). The *A*-site order stabilizes AFM(A) state associated with a $d_{x^2-y^2}$ orbital order (layer type), because the layer type order of R/Ba and consequently the distorted MnO_6 octahedra introduce 2-dimensionality in the crystal structure. The increase of the *A*-site disorder makes AFM(A) state unstable because of the decrease of structural anisotropy (2-dimensionality). On the other hand, it is advantageous to FM state generated by an isotropic double exchange interaction and it leads to FM state for PB32 and PB25. However, the effect of σ^2 is simultaneously enhanced by the *A*-site disorder and finally results in magnetic glassy state in the disordered form PB00. In conclusion the *A*-site randomness in Ba-based manganites clearly suppresses not only FM transition but also AFM(A) transition and leads to magnetic glassy state. We observed a similar randomness effect on Nd-compounds. Previously Akahoshi *et al.*[11] reported somewhat different result of FM states as the ground state for $Pr_{0.5}Ba_{0.5}MnO_3$ and $Nd_{0.5}Ba_{0.5}MnO_3$. The present experiments suggest insufficient disorder in their samples.

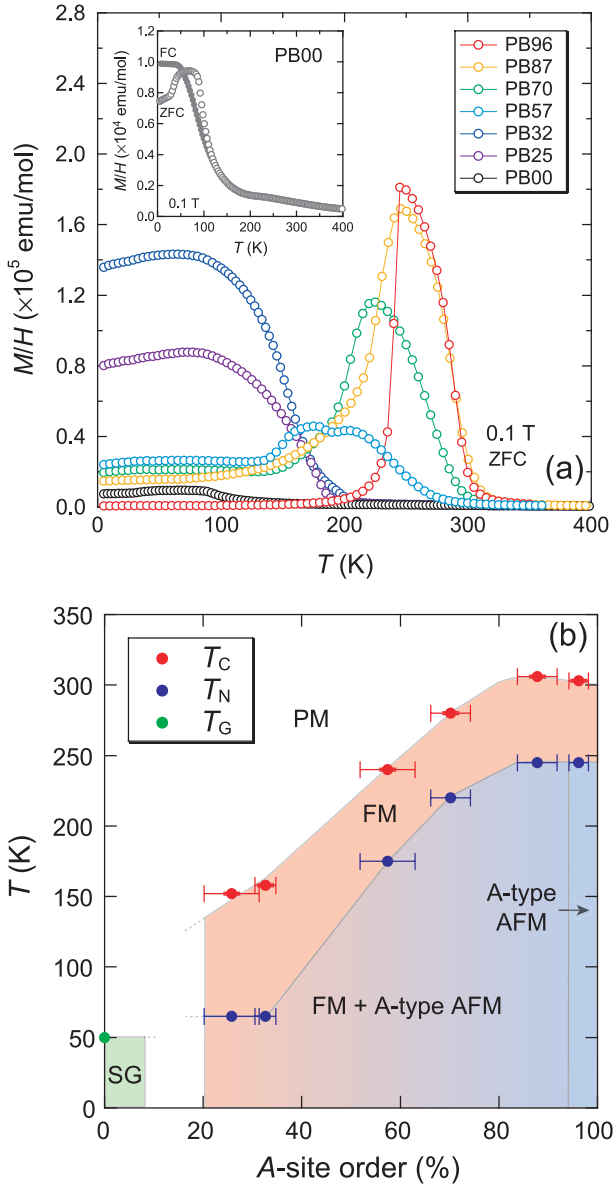

Fig. 10. (a) Temperature dependence of magnetic susceptibility for Pr-compounds (PB96–PB00) under 0.1 T. (b) Phase diagram for Pr-compounds as a function of the degree of the *A*-site order (%).

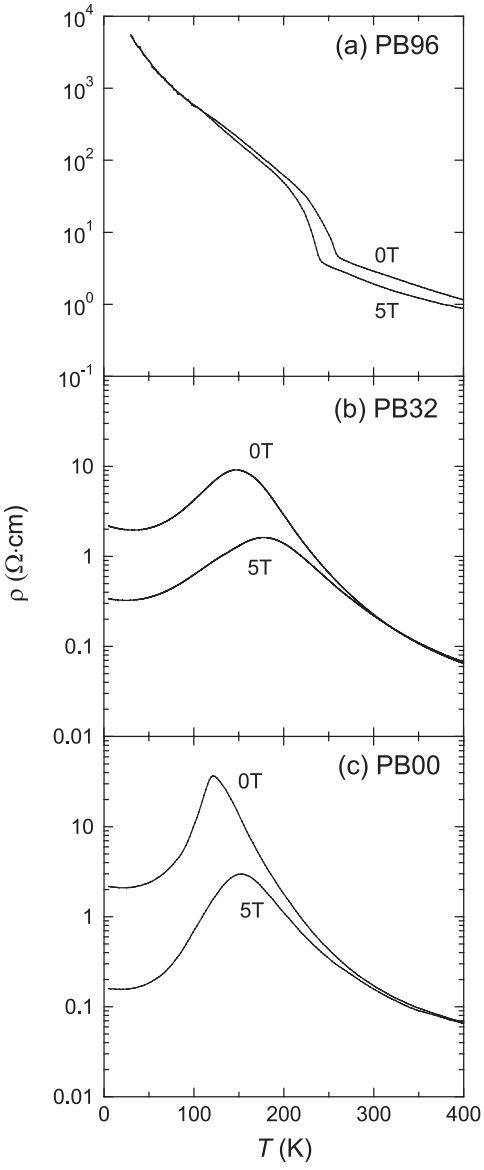

Fig. 11. Temperature dependence of electrical resistivity at 0 and 5 T for (a) PB96, (b) PB32 and (c) PB00.

Figure 11 shows temperature variation of electrical resistivity ρ in (a) PB96, (b) PB32 and (c) PB00 at 0 and 5 T. For PB96 in which AFM(A) state is stable, magnetic field dependence of resistivity is little, although AFM(A) transition temperature is obviously suppressed by 18 K at 5 T. On the other hand, magnetoresistance (MR) effect is observed below T_C (= 158 K) for ferromagnetic PB32 and below 120 K even for PB00 which has no long-range ferromagnetic order. The MR effects of these compounds at 5 T are summarized in Fig. 12, where MR (%) is given by MR (%) = $\{[\rho(0) - \rho(H)]/\rho(0)\} \times 100\%$ with $\rho(H)$ in 5 T and $\rho(0)$ in zero magnetic field. With increasing the *A*-site randomness, MR effect increases and the maximum MR effect reaches to 2360% in PB00, although the temperature (T_{MR}) at the maximum MR effect decreases. It is obvious that the *A*-site randomness increases MR effect in Pr-compounds. This is the first observation of the efficient MR effect caused by the *A*-site disorder in a series of compounds

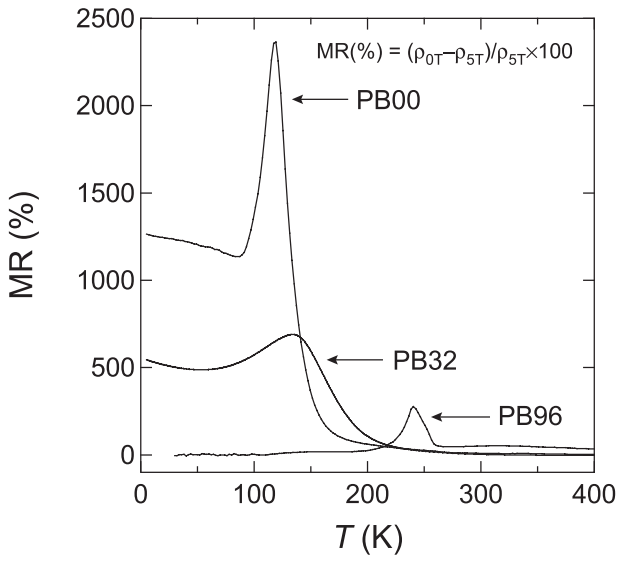

Fig. 12. Magnetoresistance (MR) vs temperature plots for PB96, PB32 and PB00. MR effect was measured between 0 and 5 T.

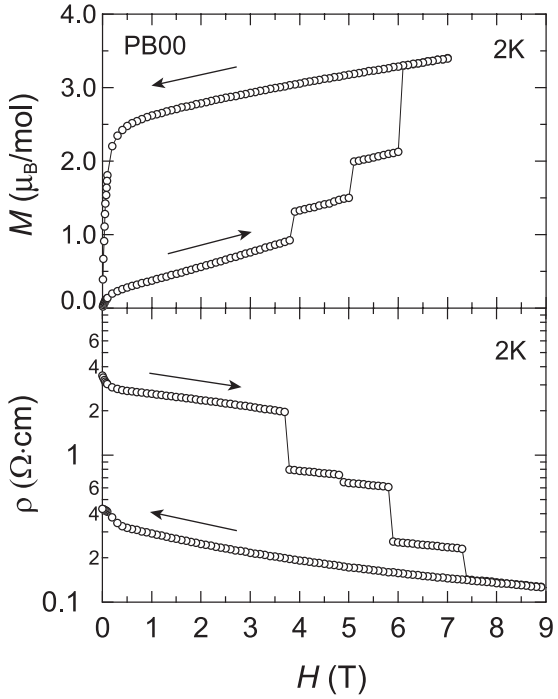

Fig. 13. Magnetic field dependences of resistivity and magnetization at 2 K for PB00.

with a fixed composition and various degrees of the *A*-site randomness. We also found very similar behaviors in Nd-compounds.

The decrease of resistivity below 150 K in PB32 is due to the development of FM state and the observed MR effect could be associated with the conversion of coexisted phases [AFM(A) phase or magnetic glassy phase] to FM phase by an external magnetic field. On the other hand PB00 shows no long range magnetic ordering nevertheless it shows similar behaviors of resistivity and MR effect. Such behaviors would be due to the development of short range magnetic ordering and the conversion of magnetic glassy phase to FM phase by an external magnetic field. At 2 K in PB00, a peculiar behavior, as shown in Fig. 13, has been observed. The resistivity decreases stepwise as the magnetic field increases, while the magnetization increases stepwise with the close relation to the resistivity behaviors. These behaviors are not reversible in the magnetic field. The stepwise behaviors in the magnetization and resistivity were observed up to 4.9 K but they vanished dramatically at 5.0 K. Similar behaviors were previously reported in $Pr_{0.5}Ca_{0.5}MnO_3$ doped with a few percent of other cations such as Sc, Ga or Co on the Mn site and were explained by an impurity induced-disorder, with the coexistence of several short-range AFI(CE) phases and small FM regions.[18,19] Our system has neither FM-to-AFI(CE) transition nor dopant in contrast to $Pr_{0.5}Ca_{0.5}MnO_3$. A model based on ordinal two-phase mixture cannot explain the behavior. For instance, AFI(CE) phase in the coexistence with FM phase is continuously converted to FM phase as observed in $LaBaMn_2O_6$.[6] We have no explanation for such multi-step magnetization and resistivity change at present. However we would like to emphasize a close relation between the observed behavior and any spatial heterogeneity in a nanometer scale. Detailed study is now in progress.

4. Summary

To summarize, we have investigated the structures and electromagnetic properties of the *A*-site disordered Ba-based manganite $R_{0.5}Ba_{0.5}MnO_3$ (R = Y and rare earth elements) and compared $R_{0.5}Ba_{0.5}MnO_3$ with not only the *A*-site ordered manganite $RBaMn_2O_6$ but also ordinary disordered manganites $R_{0.5}A_{0.5}MnO_3$ (A = Ca and Sr). The disordered form $R_{0.5}Ba_{0.5}MnO_3$ has a primitive cubic perovskite cell with no tilt of MnO_6 octahedra. The electronic states characteristic of perovskite manganites are absent in $R_{0.5}Ba_{0.5}MnO_3$ and magnetic glassy states govern the electronic state of $R_{0.5}Ba_{0.5}MnO_3$. The magnetic glassy states could be due to the disorder effect that hinders the long-range magnetic ordering and could occur as a result of the competition between randomly distributed ferromagnetic and antiferromagnetic interactions. The *A*-site randomness effect has been investigated in Pr-compounds with various degrees of Pr/Ba randomness at the *A*-sites. The *A*-site randomness suppresses both ferromagnetic and *A*-type antiferromagnetic transitions in $PrBaMn_2O_6$. On the other hand, magnetoresistance effect becomes remarkable with increase of the *A*-site disorder. As remarkable phenomena, multi-step magnetization and resistivity changes have been observed in $Pr_{0.5}Ba_{0.5}MnO_3$. Since the ionic radius of Ba^{2+} is much larger than that of Sr^{2+} and also R^{3+}, $R_{0.5}Ba_{0.5}MnO_3$ could include any spatial heterogeneity in a nanometer scale, which could be closely related to the multi-step magnetization and resistivity changes observed.

Acknowledgements

The authors thank T. Yamauchi, M. Isobe, Y. Matsushita, H. Kageyama and K. Ueda for valuable discussion. This work is partly supported by Grants-in-Aid for Scientific Research (No. 407 and No. 758) and for Creative Scientific Research (No. 13NP0201) from the Ministry of Education, Culture, Sports, Science and Technology.

1) See reviews, C. N. R. Rao and B. Raveau: *Colossal Magnetoresistance, Charge Ordering and Related Properties of Manganese Oxides* (World Scientific, Singapore, 1998).
2) T. Nakajima, H. Kageyama and Y. Ueda: J. Phys. Chem. Solids **63** (2002) 913.
3) T. Nakajima, H. Kageyama, H. Yoshizawa and Y. Ueda: J. Phys. Soc. Jpn. **71** (2002) 2843.
4) H. Kageyama, T. Nakajima, M. Ichihara, Y. Ueda, H. Yoshizawa and K. Ohoyama: J. Phys. Soc. Jpn. **72** (2003) 241.
5) T. Nakajima, H. Kageyama, M. Ichihara, K. Ohoyama, H. Yoshizawa and Y. Ueda: J. Solid State Chem. **177** (2004) 987.
6) T. Nakajima, H. Kageyama, H. Yoshizawa, K. Ohoyama and Y. Ueda: J. Phys. Soc. Jpn. **72** (2003) 3237.
7) F. Millange, V. Caignaert, B. Domengés, B. Raveau and E. Suard: Chem. Mater. **10** (1998) 1974.
8) S. V. Trukhanov, I. O. Troyanchuk, M. Hervieu, H. Szymczak and K. Barner: Phys. Rev. B **66** (2002) 184424.
9) M. Uchida, D. Akahoshi, R. Kumai, Y. Tomioka, T. Arima, Y. Tokura and Y. Matsui: J. Phys. Soc. Jpn. **71** (2002) 2605.
10) T. Arima, D. Akahoshi, K. Oikawa, T. Kamiyama, M. Uchida, Y. Matsui and Y. Tokura: Phys. Rev. B **66** (2002) 140408.
11) D. Akahoshi, M. Uchida, Y. Tomioka, T. Arima, Y. Matsui and Y. Tokura: Phys. Rev. Lett. **90** (2003) 177203.
12) H. Aliaga, D. Magnoux, A. Moreo, D. Poilblanc, S. Yunoki and E. Dagotto: Phys. Rev. B **68** (2003) 104405.
13) Y. Motome, N. Furukawa and N. Nagaosa: Phys. Rev. Lett. **91** (2003) 167204.

14) F. Izumi and T. Ikeda: Mater. Sci. Forum **321–324** (2000) 198.
15) R. D. Shannon and C. T. Prewitt: Acta Crystallogr., Sect. B **25** (1969) 925.
16) L. M. Rodriguez-Martinez and J. P. Attfield: Phys. Rev. B **54** (1996) 15622.
17) T. Terai, T. Sasaki, T. Kakeshita, T. Fukuda, T. Saburi, H. Kitagawa, K. Kindo and M. Honda: Phys. Rev. B **61** (2000) 3488.
18) S. Hébert, V. Hardy, A. Maignan, R. Mahendiran, M. Hervieu, C. Martin and B. Raveau: J. Solid State Chem. **165** (2002) 6.
19) R. Mahendiran, A. Maignan, S. Hébert, C. Martin, M. Hervieu, B. Raveau, J. F. Mitchell and P. Schiffer: Phys. Rev. Lett. **89** (2002) 286602.